AIAA JOURNAL
Vol. 47, No. 11, November 2009

Effects of Meteorological Variability on Sonic Boom Propagation from Hypersonic Aircraft

Alexandra Loubeau* and François Coulouvrat†
Institut Jean Le Rond d'Alembert, Université Pierre et Marie Curie, 75252 Paris Cedex 05, France

DOI: 10.2514/1.41337

A numerical study of primary sonic boom propagation from a hypersonic Mach 6 cruise aircraft is performed, including the effects of nonlinearity, atmospheric absorption and dispersion, and atmospheric stratification. A second-order split-step algorithm alternating between the time domain for nonlinearity and the frequency domain for absorption allows for a faster convergence of results than conventional first-order algorithms. Daily variability of meteorological parameters is used to investigate the variability of sonic boom shock overpressure, rise time, and carpet width over the span of a year. Two locations are chosen based on their difference in climates, especially humidity, and two flight directions are considered. It is found that sonic boom rise time is especially susceptible to variability in humidity, whereas shock overpressure and carpet width are most sensitive to winds. A statistical analysis and comparison between hypersonic and supersonic aircraft configurations reveal that all sonic boom characteristics are highly dependent on the aircraft and flight conditions, so that generalizations of statistics cannot be made.

I. Introduction

AIRCRAFT flying at supersonic speeds cause the formation of shock waves that travel through the atmosphere to the ground [1]. The resultant sonic booms have characteristics that depend on the aircraft source and the atmosphere. The aircraft size, shape, speed, and flight altitude all affect the sonic boom signature.

Meteorological parameters along the wave propagation path (such as temperature, humidity, and wind) determine the nonlinear distortion, absorption, and refraction that the shock wave experiences. Variability in these meteorological parameters with location and time therefore causes appreciable variation in sonic boom characteristics.

Meteorological effects on aircraft sonic boom propagation were investigated in the 1960s, and a review from that era by Garrick and Maglieri [2] noted the complexity of atmospheric effects and presented a statistical approach to analyzing variations in measured sonic booms. Numerical modeling of sonic boom propagation was also developed by Hayes et al. [3] for a horizontally stratified atmosphere that accounted for a moving heterogeneous medium. Research in this area was continued with the implementation of atmospheric absorption and dispersion in several algorithms [4] that have demonstrated the large influence of humidity on sonic boom rise times.

Neither comprehensive measurements nor numerical predictions of the variability of sonic booms from a hypersonic aircraft have been performed to date. Although many measurements of sonic booms from supersonic aircraft are available [1,5–7], they do not assess seasonal variability nor differences due to geographical location. In addition, it is not possible to extend these results to the higher altitudes and pressure levels associated with hypersonic cruise flight. Several numerical predictions of sonic boom variability from realistic aircraft have been performed [8–11], although all have been simulated for lower Mach numbers than what is being considered in the present study.

This paper investigates the sonic boom ground impact for an aircraft flying at Mach 6 cruise at a 28 km altitude. Sonic boom impact is estimated in terms of the peak overpressure at the vertical of the flight track, the front shock rise time, and the lateral extent of the geometrical carpet. The first two parameters provide an estimation of the loudest boom likely to induce maximum annoyance, and the third parameter estimates the lateral impact of the boom during the cruise phase. As a sonic boom propagates over long distances, it is strongly affected by the atmosphere and thus is dependent on meteorology and geographical location. The impact is quantified statistically, based on numerical simulations using an extensive meteorological database.

A numerical study of primary sonic boom propagation from the Mach 6 aircraft is performed, including the effects of nonlinearity, absorption and dispersion, and stratification. Tests of accurate numerical parameters for varying strengths of nonlinearity and absorption are performed to determine the most efficient alternatives. An extended absorption model is adopted that accounts for changes in the atmosphere up to the high flight altitude required by Mach 6 operation. The effects of meteorological variability on sonic boom propagation are investigated by considering the climate at two different geographical locations over the course of a year at a 6 h resolution. Vertical gradients of meteorological parameters at a coastal area with high ground humidity are juxtaposed with those for a desert region. Key sonic boom parameters are compared with predictions for other aircraft configurations at Mach 1.6 and with a previous study for a Mach 2 aircraft [9].

Section II presents the meteorological data. In the following Sec. III, an extended absorption model is presented to take into account the high flight altitudes (about 30 km) for the Mach 6 case. Modifications to include high-altitude sound absorption in the sonic boom code are briefly presented. A brief explanation of the theory behind the sonic boom algorithm is outlined in Sec. IV, and Sec. V presents the specific parameters used in the simulations. Sonic boom predictions at the ground level are synthesized and compared with other cases and previous studies in Sec. VI.

II. Meteorological Data

Meteorological data are obtained from the European Centre for Medium-Range Weather Forecasts (ECMWF) 40-year European reanalysis (ERA-40) database [12]. Two locations are chosen based on their differences in climates, especially humidity, because atmospheric absorption was highly dependent on this parameter. The

Received 30 September 2008; revision received 24 June 2009; accepted for publication 10 July 2009.

*Centre National de la Recherche Scientifique, Unité Mixte de Recherche 7190, 75005 Paris, France; Currently Research Aerospace Engineer, NASA Langley Research Center, Mail Stop 463, Hampton, VA, 23681; aloubeau@gmail.com.

†Research Director, Centre National de la Recherche Scientifique, Unité Mixte de Recherche 7190, Case 162, 4 Place Jussieu, 75005 Paris, France; francois.coulouvrat@upmc.fr. Member AIAA.

first location, Le Havre, France, is chosen because it was at the beginning of the Concorde's supersonic flight path for the route from Paris to New York [10]. In addition, Le Havre is a coastal city that generally has a high humidity. Many sonic boom experiments have been realized at the second location, Edwards Air Force Base, California [6,13], and its desert location assures low humidities for most of the year. The ECMWF data locations closest to these two locations are chosen, and the points lay less than 60 km away from the target locations. The differences in climate between the desired and actual locations are likely small, and the ECMWF data still retain the meteorological characteristics desired for comparisons.

Existing data and predictions could possibly be compared with this project's predictions in the future. The variation in climate at each of these two locations as a function of height above ground is essential in order to estimate sonic boom propagation from high altitudes. In addition, the diurnal and yearly variations in climate at each of the two locations gives a range of conditions for study with sonic boom propagation. The year 1993 was selected based on a previous study [10] that determined that the weather for this year exhibited some near-average behavior, at least over the North Atlantic Ocean. The data types of interest include temperature, humidity, and wind velocity and direction as functions of altitude.

At Le Havre near the ground, the temperatures are warmer in the summer months, but the change with seasons is not dramatic at the ground. The temperature drops as altitude increases to about 10 km. The temperature then increases, starting around 30 km. Variations in wind direction are observed. At high altitudes, however, the predominant wind direction is W–E in the winter and E–W in the summer. High winds in excess of 150 m/s are observed at high altitudes during the winter. The S–N wind velocity exhibits many variations between northerly and southerly directions and an intensification near 10 km. The relative humidity is high close to the ground and drops off sharply to 0% at around 13 km. It does not, however, increase from 15 to 30 km and decrease again as expected from the standard models [14].

In contrast to Le Havre, Edwards exhibits a large range of temperature variations. Near the ground, the temperatures are much higher in the summer through early October, reaching up to 315 K, as expected for a desert location. The lowest temperatures are found around 17 km. There are light easterly winds near the ground and strong westerly winds near 10 km. As with Le Havre, at higher altitudes, westerly winds dominate in the winter and easterly winds prevail in the summer. The S–N velocity direction varies between northerly and southerly, and some of the strongest winds occur near 10 km. The relative humidity shows a relatively dry climate (even near the ground) for most of the year, with only January and February being humid. The decrease in humidity near 13 km is less regular than for Le Havre, especially during the summer months. As with Le Havre, the relative humidity remains at 0% at high altitudes.

III. Atmospheric Absorption Model

The definition of atmospheric absorption at high altitudes is important for determining propagation of sonic booms from hypersonic aircraft and propagation of secondary sonic booms, which initially travel upward. The current International Organization for Standardization [15] and American National Standards Institute (ANSI) [16] standards, however, describe atmospheric absorption only up to 20 km. The basic absorption equations outlined in the standards require modifications at high altitudes due to changes in the chemical composition of the air. For example, molecular vibrational relaxation near the ground is attributed to relaxation of diatomic oxygen O_2 and nitrogen N_2, and the contribution from other molecules is considered insignificant. At higher altitudes, however, molecular vibrational relaxation of carbon dioxide CO_2 and ozone O_3 can reach significant levels. New algorithms by Sutherland and Bass extend atmospheric absorption predictions to higher altitudes [14,17].

Absorption in the range of altitudes 0–30 km is of interest for the current study, and absorption at higher altitudes should be considered for secondary sonic boom propagation. Therefore, it appears that carbon dioxide relaxation should be considered in the absorption calculations. It can be seen that classical absorption begins to dominate the total absorption in the same range at which carbon dioxide relaxation becomes strong; therefore, the effect of carbon dioxide is limited to a small range, which depends on frequency. The effect on the total absorption, although small, is seen in the transition region in which vibrational relaxation loss is being overtaken by classical absorption. The difference is most noticeable at low frequencies, which correspond to the fundamental frequency of sonic booms.

Atmospheric dispersion is also considered, and it is found that dispersion due to classical and rotational relaxation effects can affect the sound speed above an altitude of approximately 60 km. At lower altitudes, dispersion due to vibrational relaxation dominates, and oxygen and nitrogen relaxation effects are sufficient to characterize this dispersion. Carbon dioxide relaxation has only a slight effect at low frequencies in a transition region of around 80–100 km and is therefore not considered here.

Extension of classical plus rotational relaxation absorption is not necessary if the maximum altitude of interest is 30 km. Even though the final effect of carbon dioxide vibrational relaxation on total absorption does not seem to be very large, it could affect sonic boom propagation in a limited range. Vibrational relaxation of ozone does not seem to be significant for the altitudes and frequencies of interest. Classical and rotational relaxation dispersion is not significant at altitudes of 30 km and below. In this range, oxygen and nitrogen relaxation dispersion are sufficient.

As a minimum, carbon dioxide relaxation absorption is considered in addition to the standard absorption and dispersion calculations for high-altitude sonic boom propagation direct to the ground. Specifically, the simplified standard equations are included for classical and rotational relaxation absorption. Vibrational relaxation of diatomic nitrogen and oxygen are also calculated from the standard equations. Additionally, carbon dioxide vibrational relaxation absorption is calculated, and all other dependent calculations are included. Dispersion due to nitrogen and oxygen relaxation is also included.

IV. Sonic Boom Algorithm

A. Theoretical Model

In the present study, sonic boom propagation is modeled using classical nonlinear ray tracing theory [18] with the addition of absorption effects. Acoustical rays are paths that minimize the propagation time between the source (the aircraft) and the observer (here, the ground level) according to Fermat's principle. The equations governing ray propagation in a moving medium may be found in Pierce [19]. Along a given ray, the pressure field p 1) varies in amplitude under the effect of the medium stratification and the convergence or divergence of acoustical rays associated with aircraft maneuvers; 2) steepens under the action of nonlinear effects that make the compression phases propagate slightly faster than the sound speed, and the expansion phases propagate slower; and 3) decays under the absorption effects described in the previous section.

The pressure can be shown [20,21] to satisfy the following equation:

$$\frac{\partial p}{\partial l} + \frac{1}{2B(l)}\frac{\mathrm{d}B}{\mathrm{d}l}p = \frac{\beta\Omega}{\rho_0 c_0^2 |c_0\mathbf{n} + \mathbf{u}_0|}p\frac{\partial p}{\partial \tau} + \mathcal{A}\left(l, \frac{\partial}{\partial \tau}\right)p \qquad (1)$$

where l is the curvilinear abscissa along a given ray; $B = |A|/(\rho_0\Omega^3)$ is the Blokhintzev invariant [22] associated with the conservation of acoustical intensity along an infinitesimal ray tube; $A(l)$ is the infinitesimal ray tube area; ρ_0, c_0, and $\mathbf{u}_0$ are, respectively, the atmospheric density, sound speed, and wind speed; $\mathbf{n}$ is the unit vector normal to the wave front; $\Omega = c_0/(c_0 + \mathbf{u}_0 \cdot \mathbf{n})$; and $\beta = (\gamma + 1)/2$ is the coefficient of nonlinearity with γ the ratio of specific heats. The variable $\tau = t - \Psi(l)$ is the retarded time, where Ψ is the eikonal function measuring the propagation time along the ray

$$\Psi = \int_0^l |c_0\mathbf{n} + \mathbf{u}_0|^{-1}\,\mathrm{d}l$$

The absorption/dispersion operator $\mathcal{A}$ is linear, frequency dependent (as symbolized by the dependency on $\frac{\partial}{\partial\tau}$), and dependent on position l (which in turn is dependent on pressure, temperature, humidity, and chemical composition). Although it is possible to write this operator explicitly [20,21,23], a frequency formulation is used here [14], as described in Sec. III. Geometrical effects can be eliminated by the following transformation:

$$q[\sigma(l),\tau] = p[\sigma(l),\tau]\sqrt{\frac{B(\sigma)}{B(0)}} \tag{2}$$

Introducing the age variable σ such that

$$\frac{\mathrm{d}\sigma}{\mathrm{d}l} = \frac{\beta\Omega}{\rho_0 c_0^2 |c_0\mathbf{n} + \mathbf{u}_0|}\sqrt{\frac{B(0)}{B(l)}} \tag{3}$$

finally yields the generalized Burgers equation under the following form, more suitable for numerical simulation:

$$\frac{\partial q}{\partial\sigma} - q\frac{\partial q}{\partial\tau} = \left(\frac{\mathrm{d}\sigma}{\mathrm{d}l}\right)^{-1}\mathcal{A}\left[l(\sigma),\frac{\partial}{\partial\tau}\right]q \tag{4}$$

where quadratic nonlinearities appear on the left-hand side (the inviscid Burgers equation), and absorption and dispersion appear on the right-hand side.

B. Numerical Algorithm

Several numerical algorithms to solve Eq. (4) have been proposed. Comparisons between the different algorithms have been documented by Bass and Raspet [24], Cleveland et al. [4], and Gainville [21]. The algorithm SHOCKN [24,25] solves the generalized Burgers equation by means of a first-order fractional split-step method, treating alternately nonlinear effects in the time domain through weak shock theory and absorption/dispersion in the frequency domain. This algorithm generalizes those of Pestorius [26] and Anderson [27], established for a plane and a spherical wave, respectively. A somewhat similar technique was developed for ZEPHYRUS [20], although it allows the steepest shocks that appear near the aircraft to be treated as discontinuities in order to avoid prohibitively high time sampling rates. Comparisons of ZEPHYRUS predictions with boom recordings from an SR-71 aircraft show reasonable agreement [7]. The software THOR [28] solves absorption and dispersion in the time domain. Space sampling is chosen adaptively and is sufficiently small, so that the nonlinear step never produces shock waves. However, to avoid lengthy computations for weak absorption or large amplitudes, additional numerical dissipation is added in this case. Recently, a second-order and full spectral algorithm has been developed for the numerical simulation of long-range secondary booms [21]. This leads a priori to a higher precision, but additional numerical attenuation is also necessary for numerical stability. Comparisons of the SHOCKN, ZEPHYRUS, and THOR algorithms [4] show very similar computed rise times at the ground level.

The algorithm used in the present study is similar in principle to ZEPHYRUS but with the following two modifications. First, weak shock theory in the inviscid case is handled through the Burgers–Hayes method [3,29–31], based on the Poisson solution of the potential instead of the pressure. According to the entropy condition, the physical solution of the multivalued continuous potential is found by simply selecting the maximum value at each point. This allows nonlinearity to be calculated without requiring small range steps and automatically handles shock formation and shock merging. This method has already been used to investigate the coupling of nonlinearity and diffraction [32–35]. Second, a second-order algorithm has been developed using Strang splitting [36], in which nonlinearity is applied over a half-range step, absorption is applied over a full step (without any additional numerical dissipation), and (finally) nonlinearity is applied over another half-range step [30]. Repeating this procedure results in two nonlinear half steps being adjacent, which effectively is the same as applying nonlinearity over a full step. The second-order algorithm therefore only differs from the first-order one by applying nonlinearity over a half step at the beginning and at the end of propagation. The additional numerical cost is very minor, but the gain is substantial: the error for the second-order algorithm is on the order of $(\Delta\sigma)^2$ instead of $\Delta\sigma$ for the first-order algorithm. The second-order algorithm thus converges much faster, allows for a larger range step, and hence requires less computation time.

The benefits of the second-order split-step method are illustrated here for the plane viscous case where the right-hand side of Eq. (4) is equal to

$$\frac{1}{\Gamma}\frac{\partial^2 q}{\partial\tau^2}$$

where Γ is the Goldberg number defining the relative strength of nonlinearity to that of absorption. Figure 1 is an example of rise time convergence with an increasing number of range steps, for an N wave propagated to $\sigma = 3$ with $\Gamma = 100$. Using only five steps, both the first- and second-order cases predict waveforms that are too steep with erroneously short rise times. The second-order algorithm, however, quickly converges to the correct rise time with a significantly smaller number of steps than the first-order algorithm. The advantage is that the second-order algorithm requires less range steps for accurate results.

This algorithm has been implemented within an existing sonic boom code [9,10,33,37,38]. The time sampling of the waveform and the propagation range step size are selected to minimize computation time and retain an accurate result. Investigations into how these parameter constraints change with the input pressure and absorption are performed, and the resulting parameter values are applied in the final algorithm.

V. Sonic Boom Computations

Sonic booms are calculated for the Mach 6 configuration, a parabolic fuselage, and a halved parabolic configuration. Different options in the code are used to calculate ground track waveforms, sonic boom carpets, and limiting rays. All calculations are done for a rigid ground and account for pressure doubling due to the ground reflection. This assumption will lead to an overestimation of sonic boom levels relative to a finite impedance ground such as grass [38].

In addition to meteorological data, the other input to the sonic boom propagation code is the aircraft waveform. The Mach 6 near-field signature at a 28 km altitude, shown in Fig. 2, is extracted from the computational fluid dynamics (CFD) results for a 200 passenger aircraft with a length of 105.1 m, a maximum fuselage height and width of 5.8 and 8.9 m, respectively, a wingspan of 29.1 m, and a

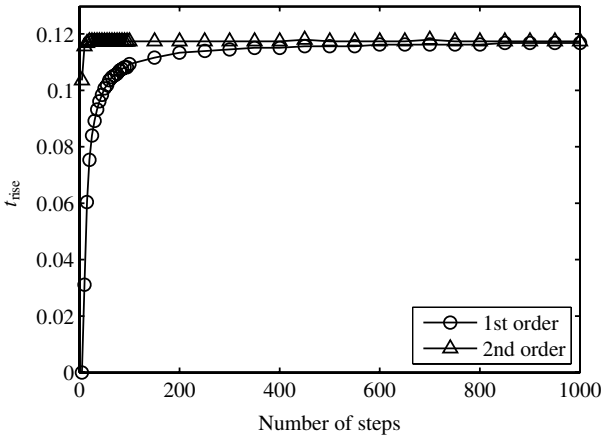

Fig. 1 Rise time convergence results for an N wave propagated to $\sigma = 3$ with $\Gamma = 100$. Comparison between first- and second-order algorithms as a function of the number of steps.

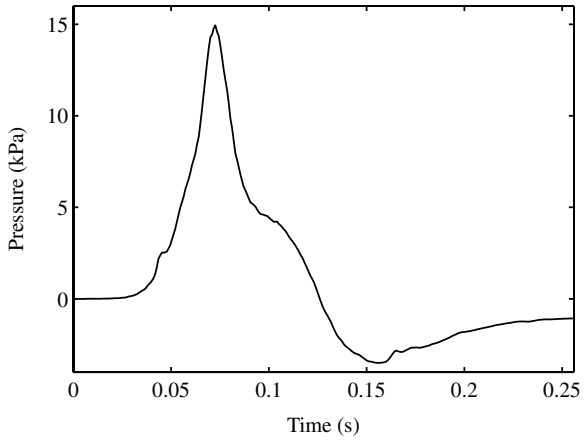

Fig. 2 Mach 6 source waveform extracted from CFD at 15.5 m ($R/L = 0.15$) for an azimuth angle of 0 deg (after multipole matching).

gross liftoff weight of 299,000 kg. The pressure signature is influenced by several shocks, caused by the nose, intake lip, nozzle flap, wing leading edges, and, to a lesser extent, the leading edges of the stabilizers. The waveform is extracted at 15.5 m from the aircraft and has multipole matching applied [39]. This short distance gives a distance-to-aircraft-length parameter of $R/L = 0.15$. This waveform may not be ideal for the acoustic code because it is extracted very close to the aircraft, therefore a ratio R/L within the range of 0.3 to 1 is usually recommended. Aircraft signatures are provided for azimuth angles of emission between 0 and 180 deg in steps of 5 deg.

The parabolic test fuselage is 45 m in length, with a volume of 141.3 m^3 and a maximum center diameter of 1.4 m. Its flight parameters are a Mach number of 1.6 and a 15 km flight altitude. For an explanation and illustration of the parabolic shape and its corresponding Whitham F function, please see Sec. 11-10 in Pierce [19]. The same fuselage with the same flight parameters is then used, with a halving of the waveform amplitude, in order to investigate separately the influence of amplitude effects. This configuration is referred to as halved parabolic. This will lead to a low-amplitude N wave at the ground level. Note that current efforts on low-boom design for supersonic business jets aim to not only reduce the amplitude, but also to incorporate boom shaping to avoid the ultimate N waveform with sharp shocks. Ground waveforms for the two additional aircraft inputs are used to compare to the Mach 6 results, especially to determine whether meteorological variability affects different waveforms in the same way.

The two parameters used to characterize the waveforms for comparison are the shock overpressure and the rise time. The shock overpressure Δp is the maximum pressure at the shock, and the rise time t_{rise} is defined as the time it takes for the amplitude to increase from 10 to 90% of the maximum. The rise time is a key parameter in sonic boom analysis because it is linked to human annoyance. The sharper the shock, the shorter the rise time, which leads to human perception of a louder, more annoying sound [40,41].

The first computations are ground track sonic booms, which result from the acoustic ray emitted at 0 deg, directly below the flight path. Calculations are made for two different flight directions, which will demonstrate the effect of winds on propagation. Sonic boom carpets are also computed using the full complement of azimuthal aircraft signatures to predict the area of ensonification at the ground.

VI. Sonic Boom Prediction Results

The Mach 6 ground track sonic boom predictions are computed only once a day due to computational limitations. The hour chosen for the Edwards calculations is 00:00 hrs coordinated universal time (UTC), or 16:00 hrs local time. At Le Havre, 18:00 hrs UTC is chosen, which corresponds to 19:00 hrs local time. The parabolic and low-boom computations, however, are completed for the full meteorological data set of four times a day.

As shown in Fig. 3, the predicted waveforms exhibit the typical N-wave shape, with a waveform spreading that has doubled the wave period for the Mach 6 case. The minimum and maximum rise time cases for the Mach 6 predictions are selected to demonstrate the differences in the shocks. These differences can be observed in Fig. 4 for the front shocks. The minimum rise time cases have sharper shocks and generally have higher shock overpressures.

A. Peak Overpressure and Rise Time

Figure 5 shows a plot of shock overpressure over time for the Mach 6 vehicle flying toward the west at Edwards. The circles are the data predicted once a day for the full year, the solid line is the mean (about 65 Pa), and the dashed lines show one standard deviation (about 1 Pa) above and below the mean. Considerable variability is observed, with slightly larger overpressures in the winter months, toward the beginning and end of the year. Figure 6 presents the same type of shock overpressure data for Le Havre. The mean shock overpressure of 65 Pa is about the same as at Edwards, and the standard deviation is about the same at 1 Pa.

The predicted rise times for the year, still for flight toward the west direction, are shown in Fig. 7 for Edwards and Fig. 8 for Le Havre. The mean rise time at Edwards is 1.7 ms, with a standard deviation of 0.7 ms. Variability is observed from below 1 to almost 5 ms, with a slight tendency toward lower rise times in the winter months, corresponding to the higher shock overpressures in the same season. This trend is due to higher humidity levels in the winter that result in less absorption near the ground. The rise times at Le Havre are shorter, due to a higher humidity than at Edwards, with a mean of 1.0 ms. The smaller standard deviation of 0.5 ms indicates that there is less variability, although there are still a few cases with much

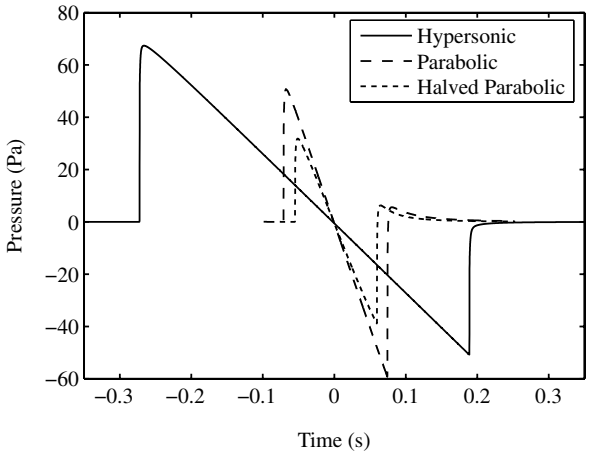

Fig. 3 Predicted sonic boom waveforms on the ground track for the three test cases and a standard atmosphere.

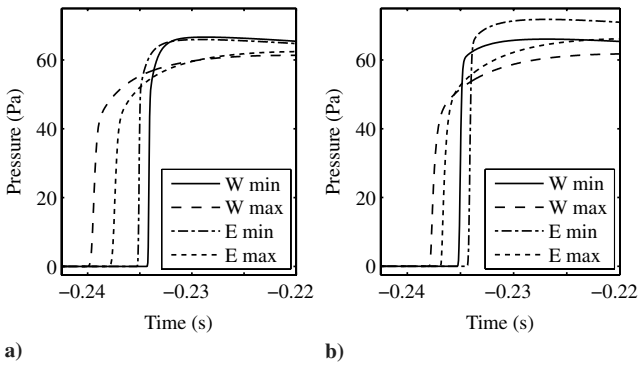

Fig. 4 Hypersonic Mach 6 predicted sonic boom front shock waveforms on the ground track for minimum and maximum rise time cases for west and east flight directions: a) Edwards and b) Le Havre.

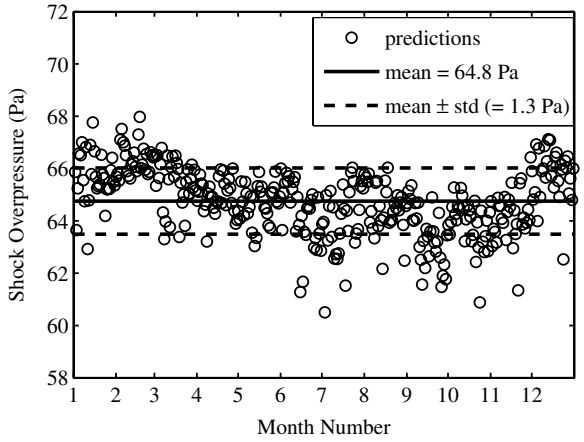

Fig. 5 Mach 6 shock overpressure at Edwards for west flight direction.

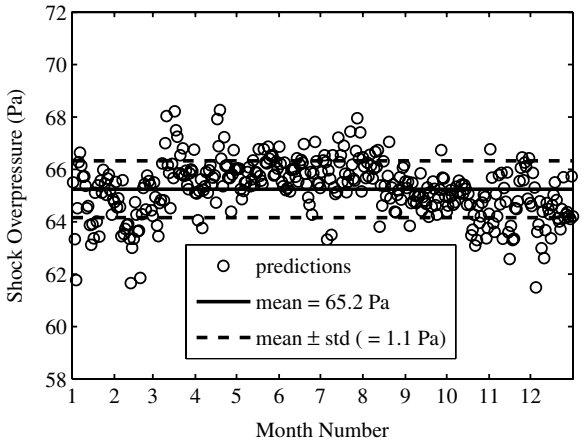

Fig. 6 Mach 6 shock overpressure at Le Havre for west flight direction.

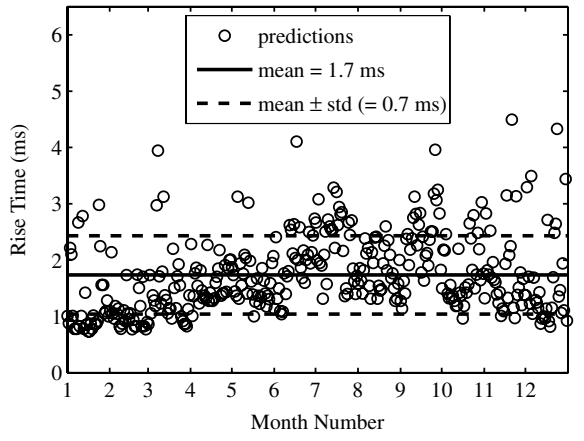

Fig. 7 Mach 6 rise time at Edwards for west flight direction.

higher rise times near 5 ms. The smaller variability in rise times at Le Havre is due to the more constant values of relative humidity close to the ground.

Table 1 summarizes all the ground track results for the three aircraft (Mach 6, Mach 1.6 parabolic, and Mach 1.6 halved parabolic). Mean values and standard deviation of the computed peak overpressure and rise time are presented for both locations and for both flight directions. As expected, the rise times decrease for each case when the humidity is higher at Le Havre. Mean rise times for the Mach 6 aircraft are 1.7 to 1.8 ms at dry Edwards, compared with 1.0 ms at humid Le Havre. The variability at Edwards is also higher

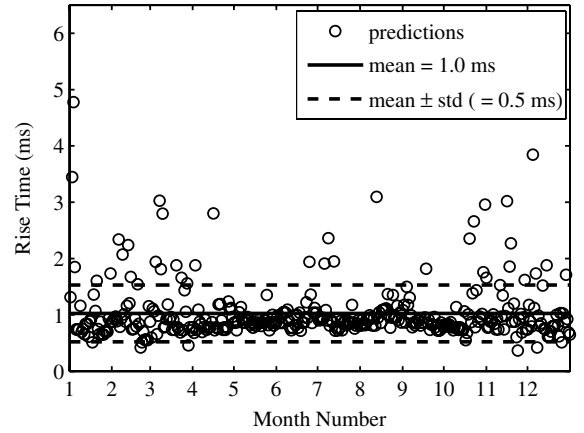

Fig. 8 Mach 6 rise time at Le Havre for west flight direction.

because of larger seasonal variations of humidity between summer (dry) and winter (humid). Flight direction does not seem to have a large effect on rise times. The shock overpressure, however, is generally a little higher for the eastward direction due to the prevailing W–E winds. Comparing different aircraft results, the pressure for the parabolic fuselage is lower than that for the hypersonic aircraft, and the halved parabolic pressure is even lower, which is expected given the difference in aircraft waveforms. For the same aircraft parameters, this decrease in pressure is associated with a corresponding increase in rise time. In general, higher pressures lead to a sharper shock with a shorter rise time.

Sonic boom recordings show a loose relationship between shock overpressure and rise time, with rise time tending to increase when pressure decreases. Some simplified asymptotic theories [42,43] indicate a rise time inversely proportional to the amplitude for a given absorption (fixed temperature and humidity). However, these theories are not applicable to sonic booms for two reasons. First, meteorological parameters, and hence sound absorption, vary significantly both with altitude and time. Second, these theories assume the sonic boom profile has reached a quasi-steady waveform (e.g., evolves near the ground like a plane wave in a uniform atmosphere). However, it is known [44] that, because of atmospheric stratification, the age variable measuring cumulated nonlinear distortion does not increase linearly, and it has an upper limit. This phenomenon, known as the freezing effect, is at the basis of the so-called Jones–Seebass–George–Darden theory [45] for low-boom design. Nevertheless, it is interesting to quantify how far sonic booms depart from the ideal case of a rise time inversely proportional to the shock overpressure.

Table 1 Comparison of predicted ground track mean rise times $\bar{t}_{\text{rise}}$, rise time standard deviations t_{std}, mean shock overpressures $\overline{\Delta p}$, and shock overpressure standard deviations Δp_{std} for the three aircraft, two locations, and two flight directions

Location	Dir.	$\bar{t}_{\text{rise}}$, ms	t_{std}, ms	$\overline{\Delta p}$, Pa	Δp_{std}, Pa
Hypersonic aircraft, Mach 6					
Edwards	W	1.7	0.7	64.8	1.3
Edwards	E	1.8	0.7	64.4	1.6
Le Havre	W	1.0	0.5	65.2	1.1
Le Havre	E	1.0	0.5	66.3	1.7
Parabolic aircraft, Mach 1.6					
Edwards	W	1.6	0.6	44.6	1.9
Edwards	E	1.5	0.6	48.6	2.4
Le Havre	W	1.0	0.4	47.8	1.5
Le Havre	E	1.0	0.4	49.8	1.6
Halved parabolic aircraft, Mach 1.6					
Edwards	W	2.2	0.8	28.0	1.4
Edwards	E	2.1	0.8	30.3	1.6
Le Havre	W	1.4	0.6	30.1	1.1
Le Havre	E	1.4	0.6	31.2	1.0

One way of examining this relationship is to compare histograms of the data. The percent occurrence of rise times, shock overpressure, and their product for the Mach 6 configuration at both locations and for both flight directions are presented in Figs. 9–12. There is a distribution of values near the mean values, presented earlier in Table 1, that demonstrate the variability of results. The rise times exhibit a variability of almost an order of magnitude, from 0.5 to 5 ms. The black dashed lines that appear for the west direction figures are the results with a standard International Civil Aviation Organization (ICAO) atmosphere [46] coupled with a mean annual relative humidity profile from Annex C of the ANSI absorption standard [16]. As shown in the histogram figures, the standard atmosphere

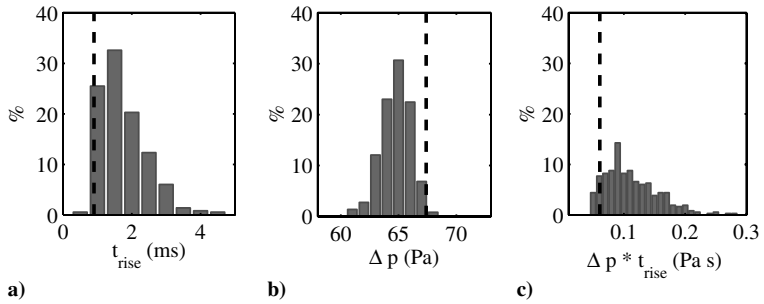

Fig. 9 Mach 6 histograms for Edwards with west flight direction: a) rise time, b) shock overpressure, and c) product of shock overpressure and rise time.

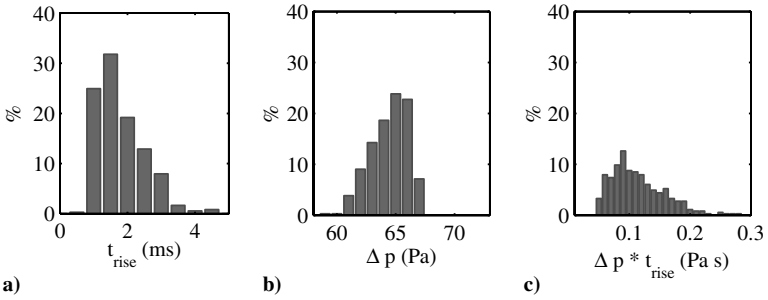

Fig. 10 Mach 6 histograms for Edwards with east flight direction: a) rise time, b) shock overpressure, and c) product of shock overpressure and rise time.

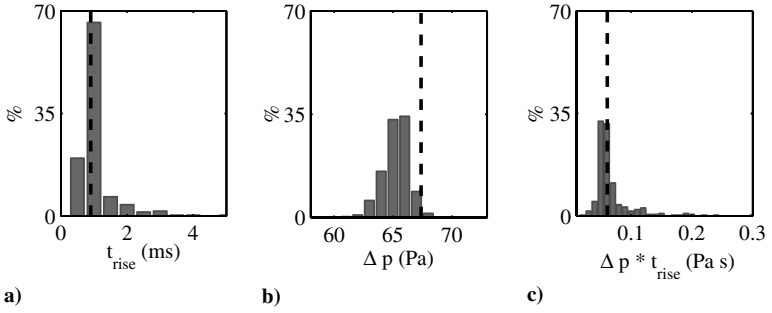

Fig. 11 Mach 6 histograms for Le Havre with west flight direction: a) rise time, b) shock overpressure, and c) product of shock overpressure and rise time.

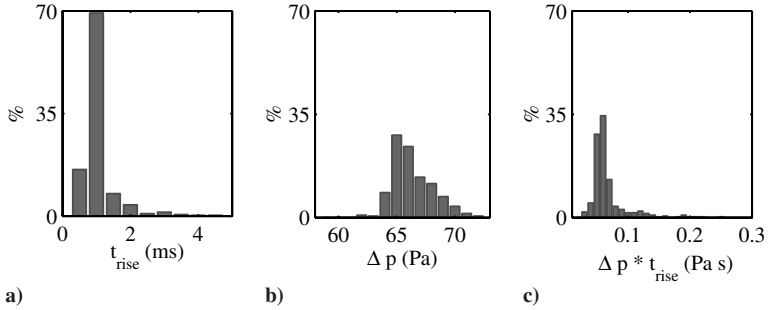

Fig. 12 Mach 6 histograms for Le Havre with east flight direction: a) rise time, b) shock overpressure, and c) product of shock overpressure and rise time.

causes rise times to be underestimated and shock overpressures to be overestimated, leading to an overestimated loudness prediction.

The statistics are completely different between Edwards and Le Havre. Note that at Edwards, the maximum percent occurrence is less than 40% for any given range, whereas at Le Havre, about 70% of the rise times are in the same range of around 1 ms. This points to a lower variability of rise times at Le Havre, which is due to the lower variability of humidity at this location. In the case of shock overpressures at Le Havre, larger pressures are predicted for the east flight direction due to W–E winds. The histograms for the product of the rise time and shock overpressure also show a large variability and, as expected, do not approach a constant. The histograms for the product also differ vastly from Edwards to Le Havre, with predictions at Edwards exhibiting a larger variability due to more variability in rise times. Although not shown here, the histograms for the parabolic and halved parabolic configurations differ greatly from the Mach 6 histograms. Hence, statistics for a given aircraft configuration cannot be extrapolated to another one.

To summarize, although peak overpressure varies by only about plus or minus 5%, extreme values of the rise time differ by almost one magnitude order, from 0.5 to 5 ms. The Edwards statistics also differ greatly from the predictions for Le Havre. Hence, rise time, for a given aircraft, is shown to be a parameter very sensitive to the local meteorology, which itself depends on the geographical location.

B. Carpet Width Predictions

Complete sets of carpet width data are computed using limiting rays for all meteorological cases. The two limiting rays define the cutoff of the sonic boom carpet at the ground. The Mach 6 carpet widths for Edwards and westbound flights show a mean carpet width of 148.4 km, with a standard deviation of 11.5 km. In contrast, the mean carpet width at the same location but for eastbound flights is larger, now at 157.3 km. The standard deviation is also larger at 15.7 km, indicating a greater variability. In a few cases, there are carpet widths that reach almost 250 km. The differences between the flight directions can be explained by considering the wind data for Edwards. Especially below 20 km, winds at Edwards are mostly eastward for the entire year. Thus, flying downwind results in a larger carpet width because of an increase in downward refraction.

For Le Havre, the mean carpet width of 160.1 km for the east direction is also larger than the 153.6 km for the west direction, and the standard deviation is also larger. In comparison to Edwards, the Le Havre carpet widths are larger, most likely due to the stronger W–E winds above 20 km at Le Havre. While varying in direction throughout the year, the S–N winds at Le Havre are also stronger than those at Edwards. With standard deviations of 19.2 and 21.1 km, there is also more variability in the carpet widths at Le Havre, which can be linked to the greater variability in wind direction below 20 km.

Histograms of the sonic boom carpet widths are included in Fig. 13. The Edwards west case, in Fig. 13a, shows the highest percent occurrence, reaching nearly 40% for a carpet width of 140 km. This relatively low variability is contrasted with the Le Havre east case, in Fig. 13d, that shows a lower percent occurrence of less than 25% at 150 and 160 km. The larger spread in results at Le Havre indicates a greater variability due to winds, and in general the predicted carpet widths are larger at Le Havre. The carpet width for a standard atmosphere (not shown) is 143 km, which is less than all the mean carpet widths predicted. The standard atmosphere therefore underestimates carpet widths, particularly for humid and windy conditions.

The same carpet width calculations were performed for the Mach 1.6 case. The carpet widths would be the same for the parabolic and halved parabolic configurations because carpet widths do not depend on aircraft shape, only on flight parameters, such as Mach number, altitude, and heading. A listing of the mean and standard deviation for each case are compared with those of the Mach 6 case in Table 2. As expected, all the Mach 1.6 carpet widths are considerably smaller than those for the hypersonic case because of the smaller Mach number and lower flight altitude. Note that the Mach 1.6 carpet widths are also much greater (almost 50% more) for eastbound

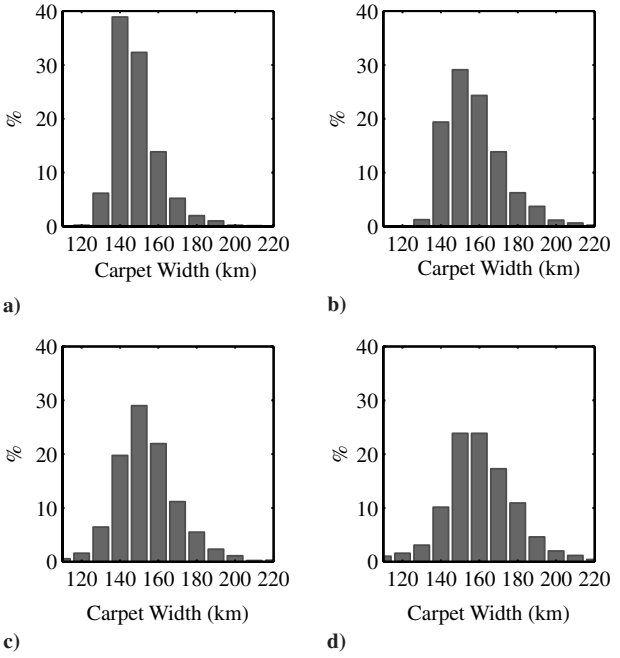

Fig. 13 Mach 6 histograms for sonic boom carpet widths: a) Edwards west, b) Edwards east, c) Le Havre west, and d) Le Havre east.

flights than for westbound flights. The Mach 1.6 carpet widths at Le Havre are also slightly larger than at Edwards and show significantly more variability. Comparisons between the two carpet widths for the two Mach cases thus show the same trends with meteorological variations, although the low Mach case exhibits much stronger dependencies due to a lower Mach number, and hence more horizontal rays that are more sensitive to wind data. One could conclude that a smaller Mach number may result in more sonic boom variability due to meteorological effects, as proposed by Blumrich et al. [10] in reference to a study of an accelerating Mach 1.2 aircraft.

C. Examples of Carpet Predictions

Sonic boom carpets are calculated for the Mach 6 vehicle once a month and for two additional special cases, resulting in 14 computations for each combination of geographical location and flight direction. The first day of each month is arbitrarily chosen, and the two special cases are the meteorological data that result in the minimum and maximum rise times for the ground track. Furthermore, the carpet is also calculated with the ICAO standard atmosphere coupled with the ANSI relative humidity profile. Each sonic boom carpet calculation involves calculation of 31 independent rays, with seven additional points for each shadow zone, if existent.

The standard atmosphere results in a symmetric carpet because no winds are included, and the remaining carpets exhibit different refraction effects due to winds, so that the extent of the carpets differs between the two sides. The carpets are mostly similar, with the largest

Table 2 Comparison of predicted mean carpet widths $\overline{cw}$ and standard deviations cw_{std} for the Mach 6 and Mach 1.6 cases, two locations, and two flight directions

Location	Direction	$\overline{cw}$, km	cw_{std}, km
	Mach 6		
Edwards	W	148.4	11.5
Edwards	E	157.3	15.7
Le Havre	W	153.6	19.2
Le Havre	E	160.1	21.1
	Mach 1.6		
Edwards	W	62.1	8.4
Edwards	E	90.3	20.2
Le Havre	W	68.5	17.0
Le Havre	E	91.3	20.5

differences occurring near cutoff and in the shadow zone, because of the variability of the carpet width previously investigated. Waveforms located in the shadow zones exhibit low amplitudes and a loss of high frequencies, leading to rounded wave shapes that are no longer N waves. The waveforms located at the carpet cutoff still retain the N-wave shape, although with much longer rise times and lower amplitudes than at the ground track. As the distance to ground track decreases, the waveforms are higher in amplitude, longer in duration, and have a steeper shock. This behavior is similar to that observed for a standard atmosphere [38]. For Le Havre, results show more differences between months than at Edwards, and this is probably due to more wind variability.

As an illustration, a few examples of carpet calculation results are given in Fig. 14, showing the shock overpressure and rise time distributions for the two selected special cases (minimum and maximum ground track rise time simulated at both Edwards and Le Havre). The aircraft flight direction is west, and the ground track situated in the middle is denoted by the vertical dashed line. Clearly visible is the pressure decrease from ground track to both the north and south sides, with an exponential decrease inside the shadow zones (when they exist for upward refraction). As a counterpart, the rise time increases gradually within the carpet and again more sharply in the shadow zone, in which it is approximately one order of magnitude larger.

D. Comparison with Previous Studies

The results of the current study are compared with that of a previous study by Blumrich et al. [9] who investigated sonic boom variability over a 10-year period (1984–1993) for three different locations. One location, St. George's Channel, is located not far from Le Havre and therefore is used for primary comparisons. The aircraft modeled was 89 m long, with a cylindrical diameter of roughly 4 m, and a 42 m wingspan. It was designed for Mach 2 cruise flight at an altitude of approximately 18–19 km. Direct comparison with the present study is not possible, but a check on the magnitude order of results and on trends is useful. The difficulty in comparison is first due to the different aircraft, Mach number, flight altitude, and assumed operating conditions. In addition, the meteorological data used were for different ranges and intervals of time. Furthermore, numerical methods with different assumptions were used to predict the ground sonic booms. Indeed, a simplified steady-state approximation [42] was used to determine the waveform at the ground, taking atmospheric absorption into account only at the ground level. As pointed out previously, this method does not yield accurate rise times because humidity variations with altitude greatly affect the rise time of a sonic boom.

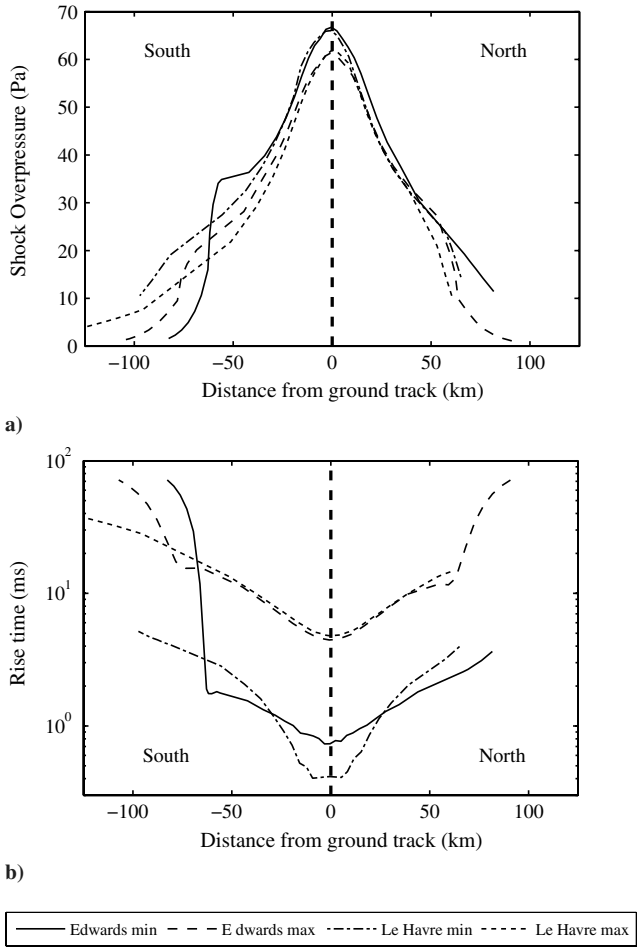

Fig. 14 Mach 6 sonic boom carpets for west flight direction and minimum or maximum ground track rise time cases at both locations: a) shock overpressure and b) rise time.

Ground track predictions for this Mach 2 aircraft vary with meteorological conditions, although seasonal variations are not easily observed. The shock overpressure variability is somewhat higher than the variability for the present predictions, although this is expected because of the longer 10-year meteorological data set. Significant differences with direction by Blumrich et al. [9] are mostly due to the application of different angles of attack, depending on distance from the takeoff airport for a given route. Variations in rise times, however, are larger for the Mach 6 configuration. This is likely related to the oversimplifying assumption of the previous study compared with the more complete model for atmospheric absorption presently applied. Directional effects on carpet widths can also be compared. Eastbound flights have larger carpet widths than westbound flights by about 10 km. This matches the trend in the present results at Le Havre, where eastbound flight has an average carpet width 6.5 km larger than for westbound flight.

VII. Conclusions

A statistical analysis of the variability of sonic booms for a Mach 6 aircraft has been performed. Aerodynamic input data are the CFD near-field computation at the distance where $R/L = 0.15$ coupled with the multipole approach. Meteorological data are extracted from the ERA-40 database of the ECMWF for the year 1993 at two geographical points near Le Havre, France, which was the beginning of the Concorde's supersonic flight between Paris and New York, and near Edwards Air Force Base, California, where most of the recent sonic boom flight tests have been performed. The two points are also characterized by a very different humidity and temperature, and hence absorption, near the ground level, due to Le Havre being on the seashore and Edwards in the Mojave Desert. The sonic boom propagation predictions include ray tracing in a stratified atmosphere with horizontal winds, nonlinear distortion, atmospheric absorption due to classical thermoviscous effects and rotational relaxation, and atmospheric absorption due to molecular vibrational relaxation of nitrogen, oxygen, and carbon dioxide.

The sonic boom emitted in the vertical plane at a 0 deg azimuth angle is computed every day for the Mach 6 configuration flying near a 28 km altitude and for two headings: west and east. The width of the geometrical carpet is also simulated systematically, along with lateral distributions calculated once per month. The ground track sonic boom reaches an amplitude of approximately 65 Pa, comparable with that of existing aircraft, most of which are comprised between 50 and 100 Pa (this last value being typical for the Concorde [5]). Because of differences in humidity, the rise time is somewhat larger at Edwards (mean value of 1.7 ms) than at Le Havre (mean value of 1.0 ms) and in both cases shows strong variability (the minimum and maximum values being separated by almost one decade). The carpet width also shows a significant variability, mostly ranging from 134 to 181 km, with larger values and more scattering at Le Havre due to stronger winds.

The present study is, to our knowledge, the only study investigating the global impact of sonic booms of a Mach 6 aircraft configuration. It shows the present configuration produces a ground sonic boom with noise characteristics (shock overpressure and rise

time) comparable with existing supersonic aircraft (like the Concorde or military aircraft) but with a wider lateral extent due to a higher Mach speed and a higher altitude. Sonic boom propagation is therefore shown to be highly dependent on the aircraft Mach speed and altitude; the geographical location, because of differences in temperature, humidity, and winds; and to a lesser extent, flight direction, due to winds. Thus, the specific aircraft model and meteorology must be used to predict sonic boom propagation. Moreover, the standard atmosphere tends to overestimate the sonic boom level at the ground.

Note that atmospheric turbulence is not included in the prediction model, and turbulence would increase the variability even further. It is believed that turbulence would generally decrease the sonic boom mean impact predicted in this paper, but it would also increase the variability.

As a conclusion, this study provides an extensive overview of the potential global impact of a given Mach 6 aircraft configuration. This study estimates that the sonic boom from this specific Mach 6 vehicle would induce at the ground a sonic boom level and rise time comparable with existing supersonic aircraft but covering a larger geographical area, due to a higher Mach speed and a higher altitude. As a consequence, overland supersonic flight by such a hypersonic vehicle is likely to be considered unacceptable by a significant proportion of the population, and hence justifies the necessity of other studies toward boom shaping and minimization with innovative aircraft designs.

Acknowledgments

This work was performed within the Aerodynamic and Thermal Load Interactions with Lightweight Advanced Materials for High Speed Flight (ATLLAS) project investigating high-speed transport. ATLLAS, coordinated by the ESA–European Space Research and Technology Centre , is supported by the European Union within the Sixth Framework Programme Priority 1.4, Aeronautic and Space, contract no. AST5-CT-2006-030729. Meteorological data were extracted from databases provided by the ECMWF. The authors wish to acknowledge ATLLAS partners DLR (German Aerospace Center) and ONERA (French Aerospace Lab) who provided the input aerodynamic data computed by computational fluid dynamics necessary for the sonic boom evaluations. The sonic boom code is used with the permission of Airbus France.

References

[1] Maglieri, D. J., and Plotkin, K. J., "Sonic Boom," *Aeroacoustics of Flight Vehicles: Theory and Practice*, edited by H. H. Hubbard, Vol. 1, Acoustical Society of America, Melville, NY, 1995, pp. 519–561.

[2] Garrick, I. E., and Maglieri, D. J., "A Summary of Results on Sonic-Boom Pressure-Signature Variations Associated With Atmospheric Conditions," NASA TN D-4588, May 1968.

[3] Hayes, W. D., Haefeli, R. C., and Kulsrud, H. E., "Sonic Boom Propagation in a Stratified Atmosphere with Computer Program," NASA CR 1299, April 1969.

[4] Cleveland, R. O., Chambers, J. P., Bass, H. E., Raspet, R., Blackstock, D. T., and Hamilton, M. F., "Comparison of Computer Codes for the Propagation of Sonic Boom Waveforms Through Isothermal Atmospheres," *Journal of the Acoustical Society of America*, Vol. 100, No. 5, 1996, pp. 3017–3027. doi:10.1121/1.417113

[5] Parmentier, G., Mathieu, G., Schaffar, M., and Johe, C., "Bang Sonique de Concorde: Enregistrement Hors Trace des Variations de Pression au Sol. Centre d'Essais des Landes; 13 au 15 Juin 1973," Inst. Franco-Allemand de Recherches de Saint-Louis, TR RT19/73, Saint-Louis, France, 1973.

[6] Lee, R. A., and Downing, J. M., "Sonic Booms Produced by United States Air Force and United States Navy Aircraft: Measured Data," U.S. Armstrong Lab., TR AL-TR-1991-0099, Wright–Patterson AFB, TX, Jan. 1991.

[7] Ivanteyeva, L. G., Kovalenko, V. V., Pavlyukov, E. V., Teperin, L. L., and Rackl, R. G., "Validation of Sonic Boom Propagation Codes Using SR-71 Flight Test Data," *Journal of the Acoustical Society of America*, Vol. 111, No. 1, 2002, pp. 554–561. doi:10.1121/1.1404377

[8] Lundberg, W. R., "Seasonal Sonic Boom Propagation Prediction," U.S. Armstrong Lab., TR AL/OE-TR-1994-0132, Wright–Patterson AFB, TX, March 1994.

[9] Blumrich, R., Coulouvrat, F., and Heimann, D., "Meteorologically Induced Variability of Sonic-Boom Characteristics of Supersonic Aircraft in Cruising Flight," *Journal of the Acoustical Society of America*, Vol. 118, No. 2, 2005, pp. 707–722. doi:10.1121/1.1953208

[10] Blumrich, R., Coulouvrat, F., and Heimann, D., "Variability of Focused Sonic Booms From Accelerating Supersonic Aircraft in Consideration of Meteorological Effects," *Journal of the Acoustical Society of America*, Vol. 118, No. 2, 2005, pp. 696–706. doi:10.1121/1.1938547

[11] Salamone, J., "Recent Sonic Boom Propagation Studies at Gulfstream Aerospace," 15th AIAA/CEAS Aeroacoustics Conference, AIAA Paper 2009-3388, 2009.

[12] Uppala, S. M., Køallberg, P. W., Simmons, A. J., Andrae, U., da Costa Bechtold, V., Fiorino, M., Gibson, J. K., Haseler, J., Hernandez, A., Kelly, G. A., Li, X., Onogi, K., Saarinen, S., Sokka, N., Allan, R. P., Andersson, E., Arpe, K., Balmaseda, M. A., Beljaars, A. C. M., van de Berg, L., Bidlot, J., Bormann, N., Caires, S., Chevallier, F., Dethof, A., Dragosavac, M., Fisher, M., Fuentes, M., Hagemann, S., Hólm, E., Hoskins, B. J., Isaksen, L., Janssen, P. A. E. M., Jenne, R., McNally, A. P., Mahfouf, J.-F., Morcrette, J.-J., Rayner, N. A., Saunders, R. W., Simon, P., Sterl, A., Trenberth, K. E., Untch, A., Vasiljevic, D., Viterbo, P., and Woollen, J., "The ERA-40 Re-Analysis," *Quarterly Journal of the Royal Meteorological Society*, Vol. 131, No. 612, 2005, pp. 2961–3012.

[13] Klos, J., and Buehrle, R. D., "Vibro-Acoustic Response of Buildings Due to Sonic Boom Exposure: June 2006 Field Test," NASA TR NASA/TM-2007-214900, Sept. 2007.

[14] Sutherland, L. C., and Bass, H. E., "Atmospheric Absorption in the Atmosphere Up to 160 km," *Journal of the Acoustical Society of America*, Vol. 115, No. 3, 2004, pp. 1012–1032. doi:10.1121/1.1631937

[15] Acoustics-Attenuation of Sound During Propagation Outdoors Part 1: Calculation of the Absorption of Sound by the Atmosphere, ISO 9613-1:1993(E), *International Organization for Standardization Handbook*, 2nd ed., Vol. 1, International Organization for Standardization, Geneva, 1993.

[16] Method for Calculation of the Absorption of Sound by the Atmosphere, American National Standards Institute, ANSI S1.26-1995 (ASA 113-1995), New York, 1995.

[17] Sutherland, L. C., and Bass, H. E., "Erratum: 'Atmospheric Absorption in the Atmosphere up to 160 km' [Journal of the Acoustical Society of America, Vol. 115, No. 3, 2004, pp. 1012–1032]," *Journal of the Acoustical Society of America*, Vol. 120, No. 5, 2006, p. 2985. doi:10.1121/1.2355481

[18] Plotkin, K. J., "State of the Art of Sonic Boom Modeling," *Journal of the Acoustical Society of America*, Vol. 111, No. 1, 2002, pp. 530–536. doi:10.1121/1.1379075

[19] Pierce, A. D., *Acoustics: An Introduction to Its Physical Principles and Applications*, Acoustical Society of America, Woodbury, NY, 1989.

[20] Robinson, L. D., "Sonic Boom Propagation Through an Inhomogeneous, Windy Atmosphere," Ph.D. Thesis, Univ. of Texas Austin, TX, 1991.

[21] Gainville, O., "Modélisation de la Propagation Atmosphérique des Ondes Infrasonores par une Méthode de Tracé de Rayons Non Linéaire, Ph.D. Thesis, Ecole Centrale de Lyon, Ecully, France, 2008.

[22] Blokhintzev, D. I., "The Propagation of Sound in an Inhomogeneous and Moving Medium 1," *Journal of the Acoustical Society of America*, Vol. 18, No. 2, 1946, pp. 322–328. doi:10.1121/1.1916368

[23] Aubin, T., and Coulouvrat, F., "Ondes Acoustiques Non Linéaires Dans un Fluide Avec Relaxation," *Journal de Mathématiques Pures et Appliquées*, Vol. 77, No. 4, 1998, pp. 387–413. doi:10.1016/S0021-7824(98)80104-9

[24] Bass, H. E., and Raspet, R., "Comparison of Sonic Boom Rise Time Prediction Techniques," *Journal of the Acoustical Society of America*, Vol. 91, No. 3, 1992, pp. 1767–1768. doi:10.1121/1.402456

[25] Bass, H. E., Ezell, J., and Raspet, R., "Effect of Vibrational Relaxation on Rise Times of Shock Waves in the Atmosphere," *Journal of the Acoustical Society of America*, Vol. 74, No. 5, 1983, pp. 1514–1517. doi:10.1121/1.390153

[26] Pestorius, F. M., "Propagation of Plane Acoustic Noise of Finite Amplitude," Applied Research Labs, TR ARL-TR-73-23, Univ. of Texas, Austin, TX, Aug. 1973.

[27] Anderson, M. O., "The Propagation of a Spherical *N* Wave in an

Absorbing Medium and its Diffraction by a Circular Aperture," Applied Research Labs, TR ARL-TR-74-25, Univ. of Texas, Austin, TX, Aug. 1974.

[28] Cleveland, R. O., Hamilton, M. F., and Blackstock, D. T., "Time-Domain Modeling of Finite-Amplitude Sound in Relaxing Fluids," *Journal of the Acoustical Society of America*, Vol. 99, No. 6, 1996, pp. 3312–3318. doi:10.1121/1.414983

[29] Burgers, J. M., "Further Statistical Problems Connected with the Solution of a Simple Nonlinear Partial Differential Equation," *Proceedings of the Royal Netherlands Academy, Series B*, Vol. 57, 1954, pp. 159–169.

[30] Coulouvrat, F., Loubeau, A., and Marchiano, R., "Shock Waves and Absorption of General Nonlinear Progressive Waves," *Proceedings of the 18th International Symposium on Nonlinear Acoustics*, edited by B. O. Enflo, C. M. Hedberg, and L. Kari, Vol. 1022, American Inst. of Physics, Melville, NY, 2008, pp. 42–45. doi:10.1063/1.2956251

[31] Coulouvrat, F., "A Quasi-Analytical Shock Solution for General Nonlinear Progressive Waves," *Wave Motion*, Vol. 46, No. 2, 2009, pp. 97–107.doi:10.1016/j.wavemoti.2008.09.002

[32] Coulouvrat, F., and Marchiano, R., "Nonlinear Fresnel Diffraction of Weak Shock Waves," *Journal of the Acoustical Society of America*, Vol. 114, No. 4, 2003, pp. 1749–1757. doi:10.1121/1.1610454

[33] Marchiano, R., Coulouvrat, F., and Grenon, R., "Numerical Simulation of Shock Wave Focusing at Fold Caustics, with Application to Sonic Boom," *Journal of the Acoustical Society of America*, Vol. 114, No. 4, 2003, pp. 1758–1771. doi:10.1121/1.1610459

[34] Marchiano, R., Coulouvrat, F., and Thomas, J.-L., "Nonlinear Focusing of Acoustic Shock Waves at a Caustic Cusp," *Journal of the Acoustical Society of America*, Vol. 117, No. 2, 2005, pp. 566–577. doi:10.1121/1.1841551

[35] Baskar, S., Coulouvrat, F., and Marchiano, R., "Nonlinear Reflection of Grazing Acoustical Shock Waves: Unsteady Transition from von Neumann to Mach to Snell–Descartes Reflections," *Journal of Fluid Mechanics*, Vol. 575, Mar. 2007, pp. 27–55. doi:10.1017/S0022112006003752

[36] Leveque, R. J., *Finite Volume Methods for Hyperbolic Problems*, Cambridge Univ. Press, Cambridge, England, U.K., 2002.

[37] Auger, T., and Coulouvrat, F., "Numerical Simulation of Sonic Boom Focusing," *AIAA Journal*, Vol. 40, No. 9, 2002, pp. 1726–1734. doi:10.2514/2.1877

[38] Coulouvrat, F., "Sonic Boom in the Shadow Zone: A Geometrical Theory of Diffraction," *Journal of the Acoustical Society of America*, Vol. 111, No. 1, 2002, pp. 499–508. doi:10.1121/1.1371973

[39] Page, J. A., and Plotkin, K. J., "An Efficient Method for Incorporating Computational Fluid Dynamics Into Sonic Boom Prediction," The 9th Applied Aerodynamics Conference, AIAA Paper 91-3275, 1991.

[40] Zepler, E. E., and Harel, F. R. P., "The Loudness of Sonic Booms and Other Impulsive Sounds," *Journal of Sound and Vibration*, Vol. 2, No. 3, 1965, pp. 249–256. doi:10.1016/0022-460X(65)90111-2

[41] Leatherwood, J. D., Sullivan, B. M., Shepherd, K. P., McCurdy, D. A., and Brown, S. A., "Summary of Recent NASA Studies of Human Response to Sonic Booms," *Journal of the Acoustical Society of America*, Vol. 111, No. 1, 2002, pp. 586–598. doi:10.1121/1.1371767

[42] Pierce, A. D., and Kang, J., "Molecular Relaxation Effects on Sonic Boom Waveforms," *Frontiers of Nonlinear Acoustics: Proceedings of the 12th ISNA*, edited by M. F. Hamilton and D. T. Blackstock, Elsevier, Amsterdam, 1990, pp. 165–170.

[43] Johnson, M. E., and Hammerton, P. W., "Effect of Molecular Relaxation Processes on Travelling Wave Solutions of Sonic Boom Waveforms," *Wave Motion*, Vol. 38, No. 3, 2003, pp. 229–240. doi:10.1016/S0165-2125(03)00044-1

[44] Hayes, W. D., "Sonic Boom," *Annual Review of Fluid Mechanics*, Vol. 3, Jan. 1971, pp. 269–290. doi:10.1146/annurev.fl.03.010171.001413

[45] Darden, C. M., "Minimization of Sonic Boom Parameters in Real and Isothermal Atmospheres," NASA TN NASA-TN D-7842, 1975.

[46] Manual of the ICAO Standard Atmosphere [extended to 80 kilometers (262,500 feet)], 3rd ed., International Civil Aviation Organization, Doc. 7488, Montreal, 1993.

M. Glauser
Associate Editor